J Biol Inorg Chem (2001) 6:390–397
DOI 10.1007/s007750100213

ORIGINAL ARTICLE

Tina M. Iverson · David M. Arciero · Alan B. Hooper
Douglas C. Rees

High-resolution structures of the oxidized and reduced states of cytochrome *c*554 from *Nitrosomonas europaea*

Received: 27 October 2000 / Accepted: 11 January 2001 / Published online: 28 March 2001

Abstract Cytochrome *c*554 (cyt *c*554) is a tetra-heme cytochrome involved in the oxidation of NH_3 by *Nitrosomonas europaea*. The X-ray crystal structures of both the oxidized and dithionite-reduced states of cyt *c*554 in a new, rhombohedral crystal form have been solved by molecular replacement, at 1.6 Å and 1.8 Å resolution, respectively. Upon reduction, the conformation of the polypeptide chain changes between residues 175 and 179, which are adjacent to hemes III and IV. Cyt *c*554 displays conserved heme-packing motifs that are present in other heme-containing proteins. Comparisons to hydroxylamine oxidoreductase, the electron donor to cyt *c*554, and cytochrome *c* nitrite reductase, an enzyme involved in nitrite ammonification, reveal substantial structural similarity in the polypeptide chain surrounding the heme core environment. The structural determinants of these heme-packing motifs extend to the buried water molecules that hydrogen bond to the histidine ligands to the heme iron. In the original structure determination of a tetragonal crystal form, a *cis* peptide bond between His129 and Phe130 was identified that appeared to be stabilized by crystal contacts. In the rhombohedral crystal form used in the present high-resolution structure determination, this peptide bond adopts the *trans* conformation, but with disallowed angles of ϕ and ψ.

T.M. Iverson · D.C. Rees (✉)
Division of Chemistry and Chemical Engineering and
Howard Hughes Medical Institute, MC 147-75 CH,
California Institute of Technology, Pasadena, CA 91125, USA
E-mail: dcrees@caltech.edu
Phone: +1-626-3958393
Fax: +1-626-7449524

D.M. Arciero · A.B. Hooper
Department of Biochemistry, Molecular Biology and Biophysics,
University of Minnesota, St. Paul, MN 55108, USA

Keywords Cytochrome · Heme · Nitrification · Porphyrin · *Nitrosomonas europaea*

Abbreviations *AMO*: ammonia monooxygenase · *cyt c552*: cytochrome *c*552 · *cyt c554*: cytochrome *c*554 · *cyt c NR*: cytochrome *c* nitrite reductase · *HAO*: hydroxylamine oxidoreductase

Introduction

Cytochrome *c*554 (cyt *c*554) is a tetra-heme cytochrome [1] involved in ammonia oxidation by the chemoautotrophic soil bacterium *Nitrosomonas europaea* [2, 3]. This transformation of ammonia represents an essential component of the process of nitrification in the biological nitrogen cycle. Oxidation of NH_3 serves as the sole energy source for *N. europaea* [4] and the physiological process proceeds through two enzymatic conversions, followed by the energy-yielding electron transfer steps. The first enzymatic step, catalyzed by the integral-membrane protein ammonia monooxygenase (AMO), converts NH_3 to hydroxylamine (NH_2OH) and water and requires the input of two electrons as well as molecular dioxygen. Following this, hydroxylamine oxidoreductase (HAO) oxidizes NH_2OH to NO_2^- at a catalytic *c*-heme that is covalently crosslinked to a protein tyrosyl residue. This latter reaction releases four electrons that are passed, possibly pairwise, to two molecules of cyt *c*554. There is controversy over the exact nature of the electron transport proteins following cyt *c*554 in vivo. Although the pathway can be reconstructed in vitro with the monoheme cytochrome *c*552 (cyt *c*552) [2], this mechanism of electron transport would bypass ubiquinone and the cytochrome bc_1 complex, which are believed to be involved in nitrification energetics in vivo. Recently, a membrane-anchored tetra-heme cytochrome (cyt c_M552) has been discovered that may act as the in vivo electron acceptor from cyt *c*554 [5].

Crystallographic studies of cyt *c*554 [6] revealed a primarily α-helical secondary structure. The four covalently attached hemes are stacked into two types of pairs. In the first type of heme pair, exemplified by hemes I/III and II/IV, the planes of each pair of porphyrin rings are nearly parallel and overlapping at the edge. Parallel heme stacking has been observed in the split-Söret cytochrome [7], HAO [8], cytochrome *c* nitrite reductase (cyt *c* NR) [9, 10], and cytochrome *c* fumarate reductase [11, 12, 13]. The second type of heme pair, exemplified by hemes III/IV, is arranged with the planes of the porphyrins nearly perpendicular to one another, as previously observed in cytochrome c_3 [14] and proteins with c_3-like repeating units [15, 16], HAO [8], and cyt *c* NR [9]. In all of these instances the protein participates in metabolic pathways requiring multiple electron transfer steps. This suggests that one function of the stacked heme motifs may be to facilitate transfer of multiple electrons required by these processes [6].

In view of the function of cyt *c*554 as a multi-electron transfer protein displaying a conserved heme arrangement, we have determined the structure in the fully oxidized and dithionite-reduced states to characterize oxidation-state-dependent conformational changes. These studies serve to identify regions of cyt *c*554 that may be functionally important for the oxidation-reduction processes required for biological nitrification, and to allow a better structural understanding of the heme packing motifs.

Materials and methods

Crystallization and data collection

Cyt *c*554 was produced, purified [17], and crystallized [6] as previously described. Instead of the tetragonal crystals produced from early preparations, one protein preparation yielded rhombohedral crystals. These crystals were of superior quality to the tetragonal crystals, with a diffraction limit up to 1.6 Å resolution. Fully oxidized crystals, grown aerobically, were reduced by adding an excess of $Na_2S_2O_4$ to the mother liquor containing the crystals. The crystals were soaked in the dithionite solution for several hours prior to cryo cooling and exhibited a subtle color change. Equivalent treatment of protein in solution resulted in four-electron reduction. Data sets were collected at –180 °C on Stanford Synchrotron Radiation Laboratories beam line 7-1 using a wavelength of 1.08 Å and a 180 mm MAR Research image plate detector.

Data processing and structure solution

Data were processed and scaled using DENZO, SCALEPACK [18], and the CCP4 suite of programs [19]. The oxidized structure was solved by molecular replacement with AMORE [20], using the structure of cyt *c*554 from the tetragonal crystal form (PDB entry 1BVB) as the search model. Since the dithionite-reduced crystals were isomorphous with the oxidized crystals, the same molecular replacement solution was subjected to additional rigid-body refinement in XPLOR [21] against the reduced data. The R_{free} was composed of 1808 randomly selected reflections (5% of the total number of reflections) from the oxidized data set (Table 1). To ensure accurate comparison of the statistics, the same set of test reflections, totaling 1242 reflections, was selected from the reduced data set.

Model building and refinement

The program O [22] was used for model building of the cyt *c*554 structure. Refinement was carried out using REFMAC [19, 23], XPLOR [21], and SHELX [24]. Maps for model building were calculated with the CCP4 suite of programs [19] and were weighted using σ_A coefficients determined in REFMAC [19, 23]. As a result of anisotropic density associated with the heme irons, the histidine ligation distances to the irons were difficult to determine using standard temperature factors when calculating maps. Thus, anisotropic temperature factors for the heme irons were refined in SHELX [24], and σ_A-weighted maps from this calculation were used to determine the iron ligation distances. The resultant distances were used as restraints in X-PLOR [21], which refined the overall protein model to significantly better geometry. Data collection and refinement statistics for the oxidized and dithionite-reduced forms of cyt *c*554, refined at 1.6 Å and 1.8 Å resolution, respectively, are summarized in Table 1. The final models for the oxidized and reduced forms of the protein contain 1988 and 1954 atoms, respectively. The difference reflects that three C-terminal residues are disordered in the reduced protein and have therefore been omitted from the model.

Results and discussion

Overall fold

The structural studies of cyt *c*554 described in this work were conducted on a new, rhombohedral crystal form with superior diffraction quality relative to the original, tetragonal crystal form. The r.m.s. deviation of the Cα atoms is 0.6 Å between the current and original structures of cyt *c*554 in the oxidized state. The structural changes occurring between the two crystal forms are primarily localized to areas of the protein either involved in crystal contacts (Fig. 1a: residues 142 to 153) or that have higher temperature factors and are therefore expected to be more mobile (Fig. 1b).

Oxidation-state-dependent structural changes

The oxidized and dithionite-reduced forms of cyt *c*554 superimpose with an r.m.s. deviation in Cα positions of 0.4 Å. Thus, upon dithionite reduction of the four hemes, the majority of the protein remains in the same conformation. However, one interesting conformational change occurs in a loop between residues 175 and 179 (Fig. 1c). This loop is positioned near hemes III and IV with His179 serving as an iron ligand to heme III. The conformational change displaces the backbone over 2 Å and may be triggered by a change in the peptide bond orientation between Met178 and His179 (Fig. 2). In the oxidized form of cyt *c*554, the carbonyl group of this peptide bond is positioned 4.7 Å from the porphyrin of heme III.

Table 1 Data collection and refinement statistics

	Oxidized	Reduced
PDB entry	1FT5	1FT6
Unit cell constants		
a=b (Å)	147.89	147.24
c (Å)	33.91	33.88
Data		
Resolution (Å)	1.6	1.8
Observations	109,601	112,676
Unique observations	35,562	24,588
Completeness (%)	97.3 (86.1)[a]	95.5 (85.9)
R_{sym}[b]	0.045 (0.174)	0.051 (0.288)
I/σ	28.0 (7.3)	28.5 (5.1)
Refinement		
R_{cryst}[c]	0.188	0.197
R_{free}[d]	0.215	0.236
Estimated coordinate error (Å)[e]	0.09	0.13
No. of free-R reflections	1808	1242
R.m.s. Δ bond lengths (Å)	0.021	0.016
R.m.s. Δ bond angles (°)	1.99	1.6
Number of atoms	1988	1954
Residues	1–211	1–208
Water molecules	142	142
Other HET atoms[f]	3 ips	1 ips, 1 dtn, 1 SO_3
Ramachandran statistics		
% Most favored	87.0	87.4
% Allowed	11.3	12.0
% Generously allowed	0.6 (Ala207)	0.0
% Disallowed	1.1 (Phe130, Lys209)	0.6 (Phe130)

[a] Numbers in parentheses indicate values for the highest resolution bin
[b] $R_{sym}=\Sigma[I_i-<I>]/\Sigma[<I>]$ where i is the ith measurement and $<I>$ is the weighted mean of I
[c] $R_{cryst}=\Sigma||F_o|-|F_c||/\Sigma|F_o|$
[d] R_{free} is the same as R_{cryst} for a selection of randomly omitted reflections
[e] Estimated coordinate error is the Cruickshank's value determined in REFMAC
[f] ips is inorganic phosphate (PO_4^{2-}) and dtn is dithionite ($S_2O_4^{2-}$); SO_3 is the oxidative breakdown product of dithionite

Upon reduction and reorientation of the Met178-His179 peptide bond, this backbone carbonyl moves to 8.3 Å from the porphyrin of heme III, with an ordered water molecule filling the position that the peptide carbonyl occupied in the oxidized state. The relative rigidity of the region between residues 175 and 179 is reflected in the low temperature factors for this loop (all <20 Å^2) in both the oxidized and reduced protein (Fig. 1b). The conformational change was also observed in three additional crystals of dithionite-reduced cyt c554, including one in the tetragonal crystal form (data not shown). These observations suggest that the observed structural changes are significant and not associated with inherent flexibility of cyt c554 in that region. This conformational change may contribute to the biphasic kinetics observed upon dithionite reduction [25].

A second conformational change associated with the reduction of cyt c554 is a change in the position of the propionate group of heme IV. The determinants of this conformational change are unclear. Other side chains that change position between the two oxidation states are located on the surface of the protein and exhibit higher temperature factors, indicating that they are conformationally more mobile. It is therefore difficult to determine whether these changes in side chain position reflect actual oxidation-state-linked changes or merely reflect conformational flexibility of these residues.

These structures show a general trend of lengthening in the heme iron-histidine nitrogen ligation distance upon reduction. This behavior is consistent with the expectation that ligand distances to ferrous iron are typically longer than for ferric iron [26]. However, the shifts in coordination distance between oxidized and reduced heme iron (Table 2) are smaller than the estimated coordinate errors in the crystal structures (Table 1), so that these changes are not statistically significant.

Although isolated porphyrins are essentially planar [27], distortions of heme porphyrins are common in proteins [28, 29]. The deviations from planarity are thought to affect the electronic structure of the heme, which in turn can alter the redox potential and ligand-binding properties [30]. Although there are exceptions, porphyrins in reduced proteins tend to be more planar than their oxidized counterparts [31, 32, 33]. In agreement with this, the hemes of the reduced form of cyt c554 exhibit less deviation from planarity than do the hemes of the oxidized form (Table 3). This change in

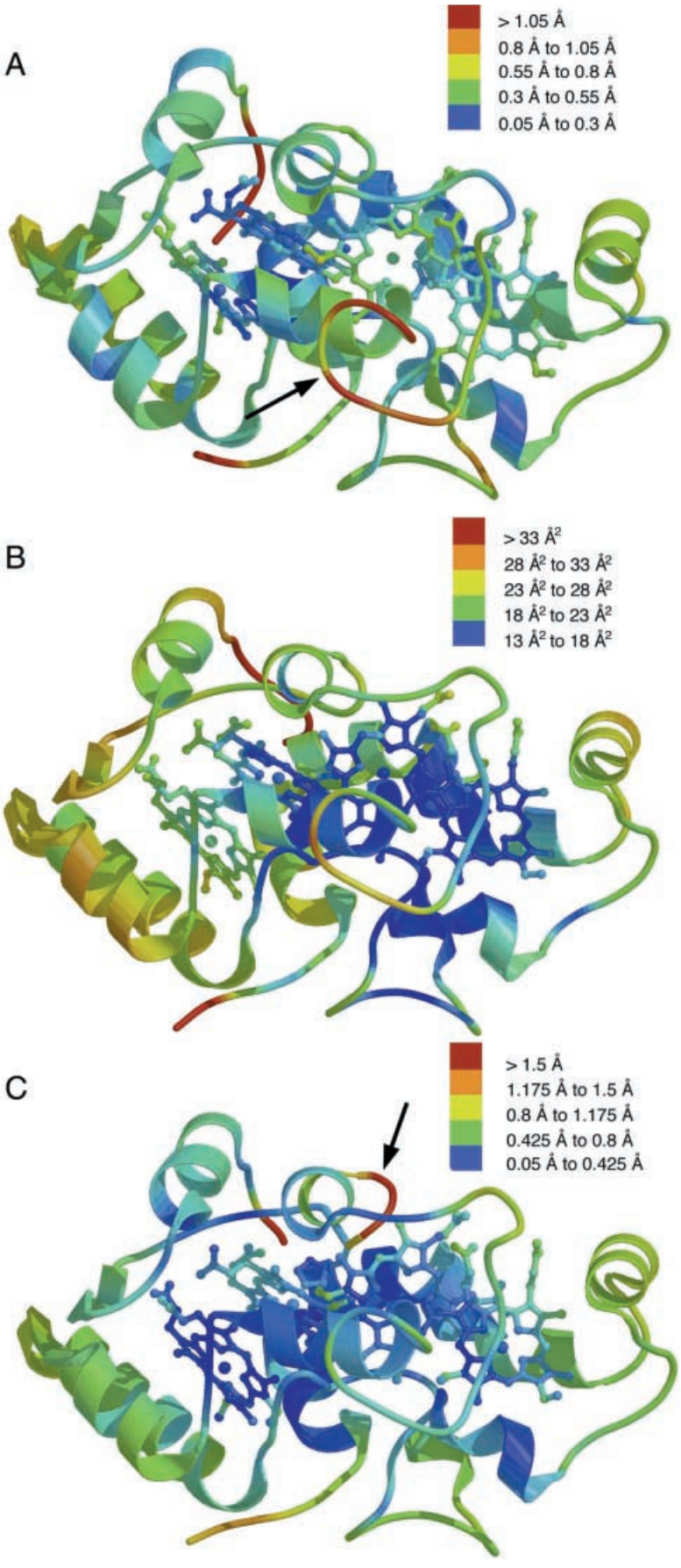

Fig. 1A–C Structural variability in cyt *c*554. **A** R.m.s. deviations between oxidized cyt *c*554 in the rhombohedral and tetragonal crystal forms. The structure of cyt *c*554 in the tetragonal crystal form is colored according to the differences between the two crystal forms, with large differences in *red*, negligible differences in *blue*, and intermediate differences scaled in *orange*, *yellow*, and *green*. The *arrow* indicates a loop between residues 152 and 153 that shifts over 1 Å between the two crystal forms that is involved in a crystal contact in the tetragonal crystal form. **B** Variation in temperature factors of cyt *c*554. The model of oxidized cyt *c*554 in the rhombohedral crystal form is colored according to the value of the temperature factors. *Red* indicates the most mobile regions of the model and *blue* indicates the most stable regions, with intermediate mobility scaled in *orange*, *yellow*, and *green*. Reduced cyt *c*554 has a similar distribution of temperature factors (data not shown). **C** Differences in oxidized and reduced rhombohedral cyt *c*554. A color scale indicating the r.m.s. deviation between the two models has been superpositioned onto the structure of reduced cyt *c*554 in the rhombohedral crystal form. The *arrow* indicates that the largest difference in C_α positions (*red*) occurs between residues 175 and 179 and maximally displaces the loop 2.3 Å. Comparison of this loop in **B** and **C** shows the nature of the conformational change with respect to the rest of the protein. All molecular representations were made using MOLSCRIPT [39], BOBSCRIPT [40], and RASTER3D [41]

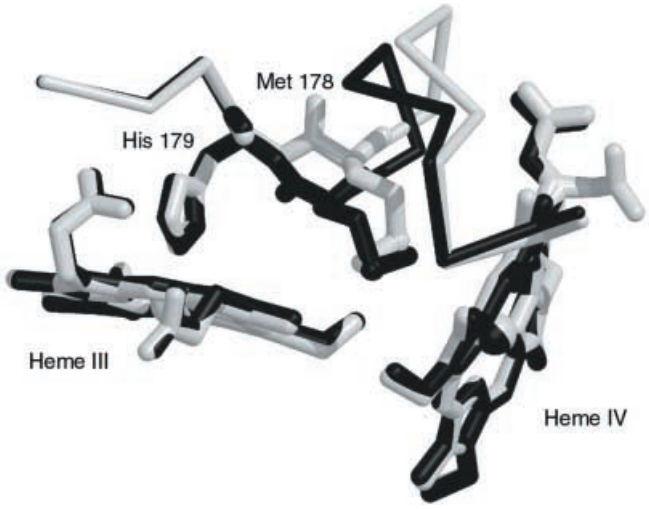

Fig. 2 Stereoview of the conformational change in the loop between residues 175 and 179. Reduced cyt *c*554 is shown in *black*, while oxidized cyt *c*554 is shown in *white*. The side chains of His179 and Met178, as well as the peptide bond between those two residues that flips upon reduction, are shown. In the structure of reduced cyt *c*554, the heme IV propionate exists in two conformations: one exhibits a position similar to that of the oxidized protein and has a calculated occupancy of 31%; the second exhibits a new position with an occupancy of 69%. Both conformations are shown

distortion is especially notable in heme IV, where the deviation from planarity decreases by over 0.3 Å upon reduction.

EPR and Mössbauer spectroscopies have shown that all four hemes of oxidized cyt *c*554 are coupled in some manner, and that this coupling decreases to unmeasurable levels as cyt *c*554 is reduced [1]. Although the close distance between the stacked hemes in cyt *c*554 suggests a structural basis for heme coupling, a difference calculation of equivalent atoms in cyt *c*554 shows that hemes I and III do not significantly change their separation upon the change in oxidation state (average of 0.02 Å further in the oxidized form). By contrast, a difference calculation of equivalent atoms of hemes II and IV shows that these two hemes have a closer average distance (0.08 Å difference) in the oxidized form. The seemingly closer separation of hemes II and IV observed in the oxidized form of the protein results from the change in heme planarity in the two oxidation states and involves atoms far from the region of direct van der Waals contact. The distance of closest approach, 3.67 Å and 3.66 Å for the C3A atoms of hemes I and III in the oxidized and reduced forms, respectively, and 3.56 Å and 3.58 Å for the C3D atoms, does not significantly change upon oxidation state for either pair of stacked hemes.

Table 2 Heme iron ligation distances (Å)

	Heme I	Heme II	Heme III	Heme IV
Oxidized proximal[a]	1.95	2.17	2.03	1.97
Oxidized distal[a]	2.08	n/a	2.01	2.03
Oxidized N_p[b]	1.98	2.03	1.99	1.97
Reduced proximal	2.00	2.20	2.04	2.06
Reduced distal	2.07	n/a	2.10	2.06
Reduced N_p	1.98	2.04	1.98	1.98

[a] Proximal refers to the histidine involved in the -C-*x*-*y*-C-H- heme binding motif, while distal refers to the histidine found elsewhere in the sequence. Heme II is five-coordinate and therefore has no distal ligand

[b] N_p refers to pyrrole nitrogen atoms and is an average of the four N_p-Fe bond lengths

Table 3 Oxidation-state-dependent porphyrin distortion (Å) from planarity[a]

	Heme I	Heme II	Heme III	Heme IV
Oxidized	0.799	0.550	0.490	0.901
Reduced	0.712	0.536	0.473	0.571

[a] Numbers represent the total distortion from planarity using a normal-coordinate structural decomposition (NSD) analysis [38]. For a detailed analysis, see http://jasheln.unm.edu/jasheln/

The heme-stacking motifs

The hemes of cyt *c*554 exhibit two types of stacking arrangements, common in bacterial multiheme *c*-cytochromes, that position the hemes within van der Waals contact [6]. The conserved stacking arrangements were shown to align cyt *c*554, HAO [8], and cyt *c* NR [9, 10] structurally [6]. This heme-based superposition demonstrates that the structural similarities extend to the conformation of the polypeptide chain surrounding the hemes [34] (Fig. 3a–c), and can be used to search for conserved side chains and solvent molecules that may be associated with the heme-stacking motif.

Although an evolutionary relatedness had previously been suggested between HAO and cyt *c* NR [35], prior to the determination of the structures of cyt *c*554, HAO, and cyt *c* NR, no significant sequence similarity had been detected between these three molecules. However, using the heme-stacking arrangement to align the polypeptide chains, evidence for sequence similarities can be detected (Fig. 3d). The similarities are weakest near the five-coordinate heme II of cyt *c*554, which corresponds to the catalytic hemes of both HAO and cyt *c* NR. The minimal sequence similarity at this heme location likely reflects the divergent functions associated with the heme counterparts.

In addition to the similarity of the polypeptide chain near the hemes, the orientation of the plane of the imidazole ring of the histidine ligand to the two perpendicular-stacked (central) hemes are similar (Fig. 4). These orientations are stabilized by hydrogen bonds to water molecules that are in conserved loca-

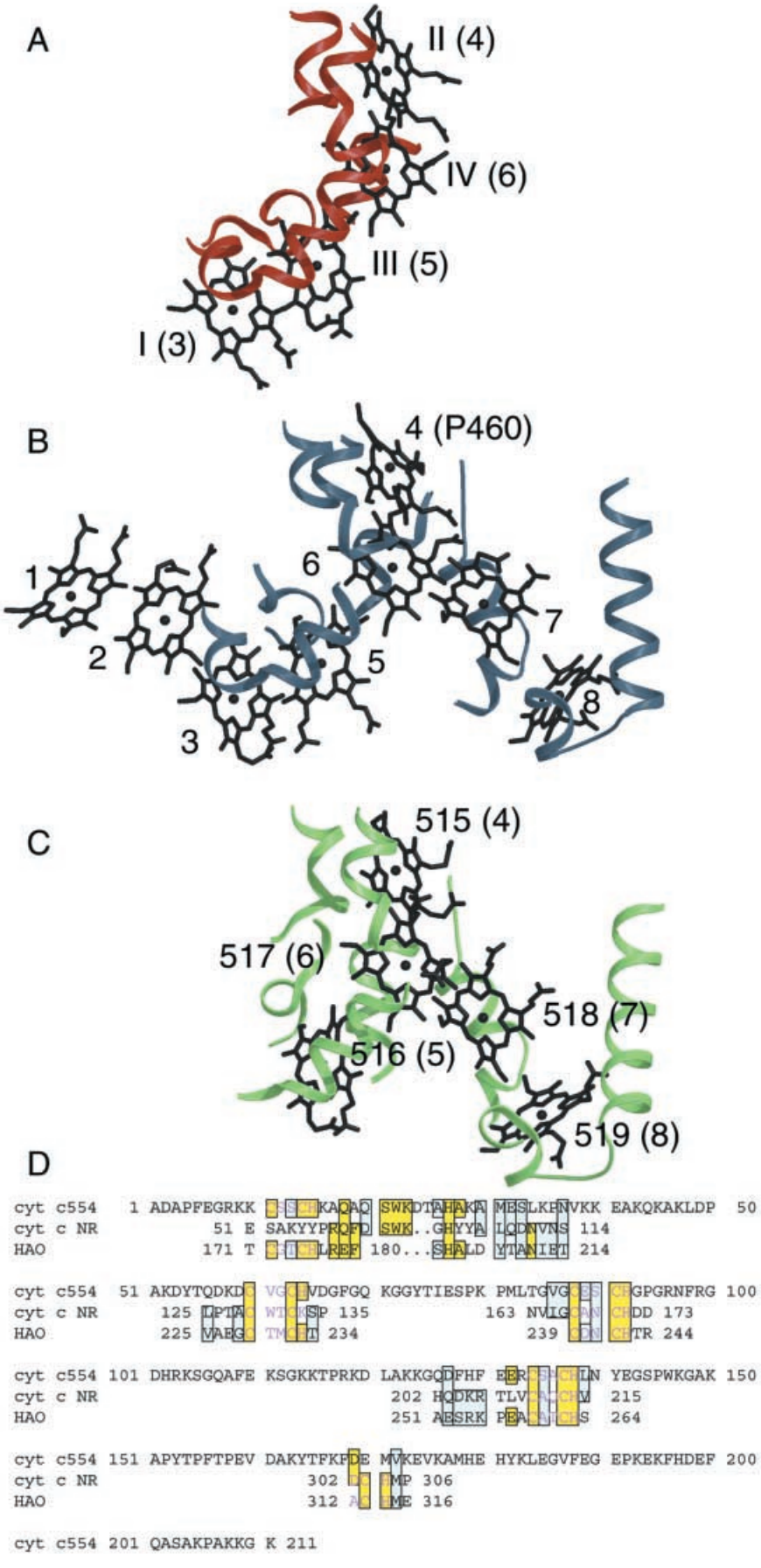

Fig. 3A–D The heme-stacking motifs. The hemes from **A** cyt *c*554, **B** HAO, and **C** cyt *c* NR are shown in the same relative orientation with surrounding secondary structural elements. The heme numbers for each are listed as well as the relative heme number from HAO. **D** A structure-based sequence alignment of cyt *c*554, HAO, and cyt *c* NR. Using the structural alignment shown in **A**–**C**, a sequence alignment has been preformed showing weak similarity of the three proteins. The sequences of the heme-binding motifs are designated with *pink text*. Regions of sequence identity are indicated with *yellow boxes*, while sequence similarity is indicated with *light blue boxes*

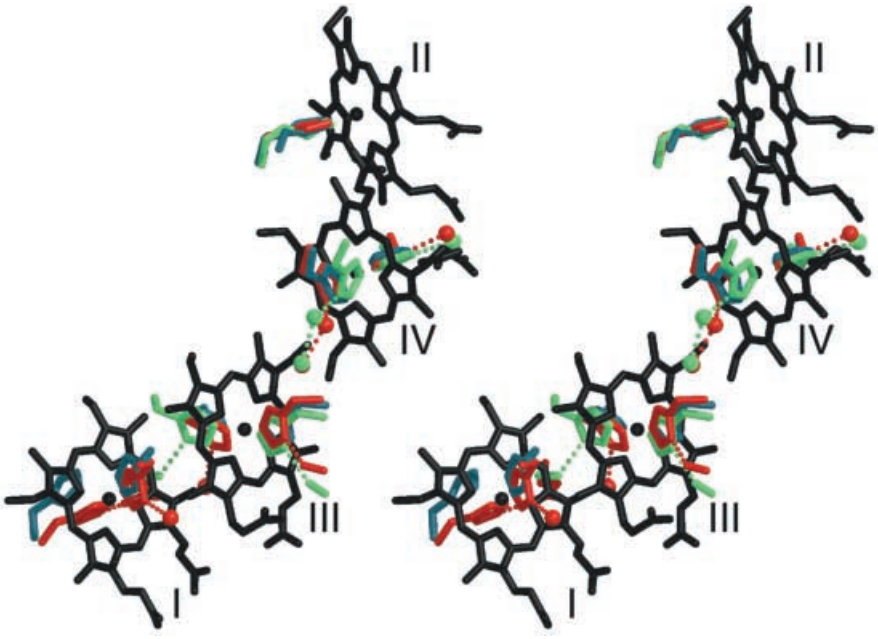

Fig. 4 Alignment of hemes common to cyt *c*554, HAO, and cyt *c* NR showing the orientation of the histidine side chain. The r.m.s. deviation of the hemes common to HAO and cyt *c*554 is 1.2 Å, while the r.m.s. deviation of the hemes common to cyt *c* NR and cyt *c*554 is 1.6 Å. Water molecules located in conserved positions are shown. Heme positions are from cyt *c*554 and are colored *black*. Side chains and water molecules from cyt *c*554 are colored *red*; those from HAO are colored *teal blue*, while those from cyt *c* NR are colored *green*

tions in the structures of both cyt *c*554 and cyt *c* NR; HAO has not been solved at a resolution where water molecules can be accurately observed. Additionally, the distal ligand to heme I of cyt *c*554 exhibits a similar orientation to heme III of HAO despite the coordination of the heme iron by the Nδ atom of His102 in cyt *c*554. Since modulation of the electronic configuration [36] of porphyrins may be affected by the orientation of the imidazole ring of the histidine ligand, the structural conservation of the side-chain orientation may reflect a component of the heme-packing motifs.

His129-Phe130 peptide bond

In the tetragonal crystal form of cyt *c*554, the bond between His129 and Phe130 adopts the *cis* conformation (Fig. 5a) [6]. This *cis* peptide bond was stabilized by a crystal contact involving the side chains of

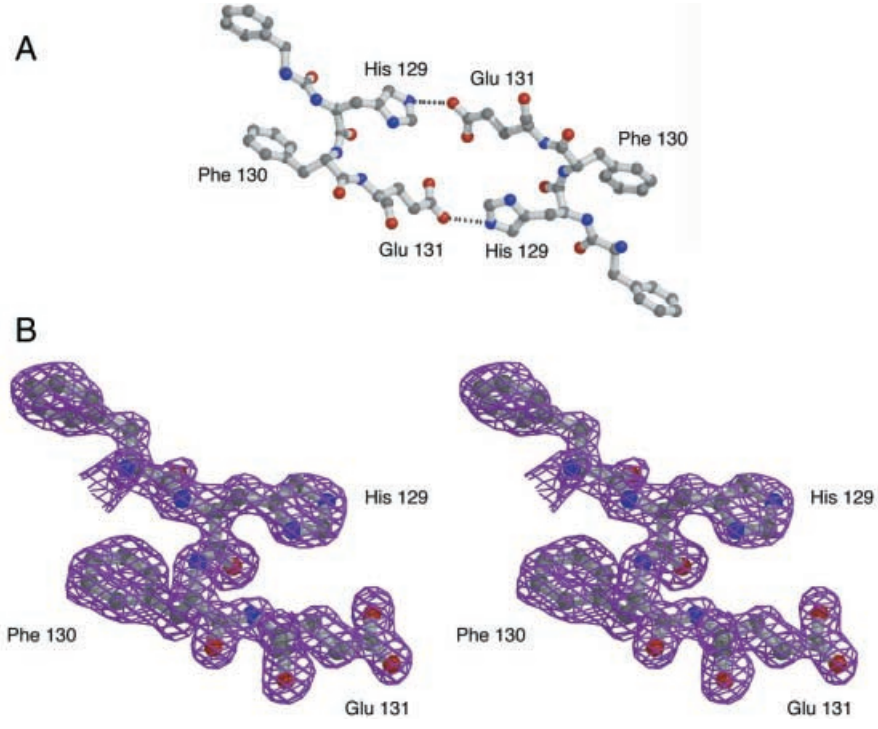

Fig. 5A, B Peptide bond at Phe130. **A** The His129-Phe130 peptide bond in the tetragonal crystal form shows a *cis* conformation, and is influenced by crystal contacts around the crystallographic two-fold axis of symmetry. **B** The His129-Phe130 peptide bond shows a *trans* conformation in the rhombohedral crystal form of the present study is shown superpositioned onto σ_A-weighted $2|F_o|-|F_c|$ density calculated after the omission of both His129 and Phe130

His129 and Glu131 around the crystallographic two-fold axis, whereas the rhombohedral crystal form has no crystal contact in this area. In both the oxidized and reduced crystals, Phe130 is in clear density and the peptide bond linking His129 and Phe130 exhibits the *trans* conformation with ϕ and ψ angles in the disallowed region of the Ramachandran diagram (Fig. 5b).

An intriguing possibility is that this peptide bond is functionally significant, with the *cis* form fortuitously stabilized in the tetragonal crystal form by crystal contacts. Crystal contacts have previously been implicated in the stabilization of functionally relevant *cis* peptide bonds for flavodoxin [37]. The location of Phe130 is in a pocket above hemes I and III near the proposed binding site for HAO [6]. Thus, isomerization of the His129-Phe130 peptide bond could be relevant for electron transfer between cyt *c*554 and HAO.

Acknowledgements We thank R. Dieckmann, J. Chiu, and F.A. Tezcan for experimental assistance and J.A. Shelnutt for calculations of the distortions of the porphyrins. This work was supported by an NSF grant (MCB-9723608) to A.B.H. and an NIH grant (GM45162) to D.C.R. T.M.I. was supported by an NIH fellowship (GM07737). This work is based upon research conducted at the Stanford Synchrotron Radiation Laboratory (SSRL), which is funded by the Department of Energy, Office of Basic Energy Sciences.

References

1. Andersson K, Lipscomb J, Valentine M, Münck E, Hooper A (1986) J Biol Chem 261:1126–1138
2. Yamanaka T, Shinra M (1974) J Biochem (Tokyo) 75:1265–1273
3. Suzuki I, Kwok S-C (1981) Can J Biochem 59:484–488
4. Wood PM (1986) In: Prosser JI (ed) Nitrification. IRL Press, Oxford, pp 39–62
5. Whittaker M, Bergmann D, Arciero D, Hooper AB (2000) Biochim Biophys Acta 1459:346–355
6. Iverson TM, Arciero DM, Hsu BT, Logan MSP, Hooper AB, Rees DC (1998) Nat Struct Biol 5:1005–1012
7. Matias PM, Morais J, Coelho A, Meijers R, Gonzalez A, Thompson A, Sieker L, LeGall J, Carrondo MA (1997) JBIC 2:507–514
8. Igarashi N, Moriyama H, Fujiwara T, Fukumori Y, Tanaka N (1997) Nat Struct Biol 4:276–284
9. Einsle O, Messerschmidt A, Stach P, Bourenkov GP, Bartunik HD, Huber R, Kroneck PMH (1999) Nature 400:476–480
10. Einsle O, Stach P, Messerschmidt A, Simon J, Kröger A, Huber R, Kroneck PMH (2000) J Biol Chem 275:39608–39616
11. Bamford V, Dobbin PS, Richardson DJ, Hemmings AM (1999) Nat Struct Biol 6:1104–1109
12. Taylor P, Pealing SL, Reid GA, Chapman SK, Walkinshaw MD (1999) Nat Struct Biol 6:1108–1112
13. Leys D, Tsapin AS, Nealson KH, Meyer TE, Cusanovich MA, VanBeeumen JJ (1999) Nat Struct Biol 6:1113–1117
14. Matias PM, Frazao C, Morais J, Coll M, Carrondo MA (1993) J Mol Biol 234:680–699
15. Matias PM, Saraiva LM, Soares CM, Coelho AV, LeGall J, Carrondo MA (1999) JBIC 4:478–494
16. Coutinho IB, Turner DL, Liu MY, LeGall J, Xavier AV (1996) JBIC 1:305–311
17. Arciero D, Collins M, Haladjian J, Bianco P, Hooper A (1991) Biochemistry 30:11459–11465
18. Otwinowski Z (1993) CCP4 study weekend data collection and processing. SERC Daresbury Laboratory, UK
19. Bailey S (1994) Acta Crystallogr Sect D 50:760–763
20. Navaza J (1994) Acta Crystallogr Sect A 50:157–163
21. Brünger AT (1992) X-PLOR version 3.1: a system for X-ray crystallography and NMR. Yale University Press, New Haven
22. Jones TA, Zou JY, Cowan SW, Kjeldgaard M (1991) Acta Crystallogr Sect A 47:110–119
23. Murshudov GN, Vagin AA, Dodson EJ (1997) Acta Crystallogr Sect D 53:240–255
24. Sheldrick GM (1990) Acta Crystallogr Sect A 46:467–473
25. DiSpirito AA, Balny C, Hooper AB (1987) Eur J Biochem 162:299–304
26. Scheidt WR, Gouterman M (1983) In: Lever ABP, Gray HB (eds) Iron porphyrins, part one. Addison-Wesley, London, pp 89–139
27. Anderson KK, Hobbs JD, Luo LA, Stanley KD, Quirke JME, Shelnutt JA (1993) J Am Chem Soc 115:12346–12352
28. Jentzen W, Ma J-G, Shelnutt JA (1998) Biophys J 74:753–763
29. Shelnutt JA, Song X-Z, Ma J-G, Jia S-L, Jentzen W, Medforth C (1998) Chem Soc Rev 27:31–41
30. Moore G, Pettigrew G (1990) Cytochromes c – evolutionary, structural and physiochemical aspects. Springer, Berlin Heidelberg New York
31. Kubitscheck U, Dreybrodt W, Schweitzer-Stenner R (1986) Spectrosc Lett 19:681–690
32. Louie GV, Brayer GD (1990) J Mol Biol 214:527–555
33. Berghuis AM, Brayer GD (1992) J Mol Biol 223:959–970
34. Iverson TM, Hendrich MP, Arciero DM, Hooper AB, Rees DC (2001) In: Wieghardt K, Huber R, Poulos TL, Messerschmidt A (eds) Handbook of metalloproteins. Wiley, New York (in press)
35. Hooper AB, Arciero DM, DiSpirito AA, Fuchs J, Johnson M, LaQuier F, Mundfrom G, McTavish H (1990) In: Gresshof PM, Newton WE, Roth WE, Stacey G (eds) Nitrogen fixation: achievements and objectives. Chapman and Hall, New York, pp 387–392
36. Shokhirev NV, Walker FA (1998) JBIC 3:581–594
37. Ludwig M, Pattridge K, Metzger A, Dixon M, Eren M, Feng Y, Swenson R (1997) Biochemistry 36:1259–1280
38. Jentzon W, Simpson MC, Hobbs JD, Song X, Ema T, Nelson NY, Medforth CJ, Smith KM, Veyrat M, Mazzanti M, Ranasseul R, Marchon JC, Takeuchi T, Goddard WA, Shelnutt JA (1995) J Am Chem Soc 117:11085–11097
39. Kraulis PJ (1991) J Appl Crystallogr 24:946–950
40. Esnouf RM (1997) J Mol Graph 15:133–138
41. Merritt EA, Murphy MEP (1994) Acta Crystallogr Sect D 50:869–873